

Article

Post-Wildfire Mobilization of Organic Carbon

Travis Numan¹, Srinidhi Lokesh¹, Abrar Shahriar¹, Anil Timilsina¹, Myron L. Lard², Justin Clark¹, Yasaman Raeofy³, Qian Zhao⁴, Simon R. Poulson⁵, Paul S. Verburg⁶, Jocelyn A. Richardson⁷, Robert L. Cook², Vera Samburova³ and Yu Yang^{1,*}

¹ Department of Civil and Environmental Engineering, University of Nevada, 1664 N. Virginia St, Reno, NV 89557, USA; tnuman@unr.edu (T.N.); slokesh@unr.edu (S.L.); shahriar1@llnl.gov (A.S.); atimilsi@umn.edu (A.T.); JustClark1305@gmail.com (J.C.)

² Department of Chemistry, Louisiana State University, 232 Choppin Hall, Baton Rouge, LA 70803, USA; mlard1@lsu.edu (M.L.L.); rlcook@lsu.edu (R.L.C.)

³ Division of Atmospheric Sciences, Desert Research Institute, 2215 Raggio Parkway, Reno, NV 89512, USA; Yasi.Raeofy@dri.edu (Y.R.); Vera.Samburova@dri.edu (V.S.)

⁴ Environmental Molecular Sciences Laboratory Pacific Northwest National Laboratory, 902 Battelle Blvd, Richland, WA 99354, USA; qian.zhao@utdallas.edu

⁵ Department of Geological Sciences & Engineering, University of Nevada, 1664 N. Virginia St, Reno, NV 89557, USA; poulson@unr.edu

⁶ Department of Natural Resources and Environmental Sciences, University of Nevada, 1664 N. Virginia St, Reno, NV 89557, USA; pverburg@unr.edu

⁷ SLAC National Accelerator Laboratory, 2575 Sand Hill Road, Menlo Park, CA 94025, USA; jocelynr@slac.stanford.edu

* Correspondence: yuy@unr.edu

Abstract: Wildfires significantly alter watershed functions, particularly the mobilization of organic carbon (OC). This study investigated OC mobility and the physicochemical characteristics of wildfire-impacted soils and ashes from the northern California and Nevada fires (Dixie, Beckworth, Caldor). Organic carbon in wildfire-derived ashes (9.2–57.3 mg/g) generally exceeded levels in the background soils (4.3–24.4 mg/g), except at the Dixie fire sites. The mobile OC fraction varied from 0.0093 to 0.029 in ashes and 0.010 to 0.065 in soils, though no consistent trend was observed between the ashes and soils. Notably, the ash samples displayed lower OC mobility compared with the soils beneath them. A negative correlation was found between the mobile OC fraction and bulk OC content. Wildfire increased the total amount of mobile OC substantially by 5.2–574% compared to the background soils. Electron paramagnetic resonance (EPR) spectra confirmed the presence of environmentally persistent free radicals (EPFRs), which correlated with observed redox reactivity. Additionally, X-ray absorption near edge structure (XANES) and X-ray fluorescence (XRF) imaging revealed that Fe(II) oxidation in soils beneath the ashes may have enhanced the OC mobility, likely driven by pyrogenic carbon and free radicals. These findings enhance our understanding of post-wildfire OC mobilization and the impact of ash–soil physicochemical properties on watershed health.

Keywords: wildfire; organic carbon; soil properties



Academic Editor: Sören Thiele-Bruhn

Received: 17 December 2024

Revised: 22 January 2025

Accepted: 24 January 2025

Published: 30 January 2025

Citation: Numan, T.; Lokesh, S.; Shahriar, A.; Timilsina, A.; Lard, M.L.; Clark, J.; Raeofy, Y.; Zhao, Q.; Poulson, S.R.; Verburg, P.S.; et al. Post-Wildfire Mobilization of Organic Carbon. *Soil Syst.* **2025**, *9*, 11. <https://doi.org/10.3390/soilsystems9010011>

Copyright: © 2025 by the authors.

Licensee MDPI, Basel, Switzerland.

This article is an open access article distributed under the terms and conditions of the Creative Commons Attribution (CC BY) license (<https://creativecommons.org/licenses/by/4.0/>).

1. Introduction

A multitude of factors arising from human activities and climate change have converged to create a significant upsurge in wildfires globally, notably in the western United States (U.S.) [1,2]. From 1984 to 2020, the area affected by forest fires increased by 1100%, further exacerbated by anthropogenic and natural climate drivers [3,4]. Wildfires, as natural moderators of terrestrial ecosystems, play crucial roles in regulating the biogeochemical

cycles of nutrients such as carbon (C) [5]. During wildfires, large amounts of organic carbon (OC) are combusted and converted to carbon dioxide (CO₂). Jones et al. [6] estimated that wildfires incinerated 256 teragram (Tg) of biomass annually, primarily producing CO₂. The greenhouse gas (GHG) emissions caused by wildfires can be partially offset by the impact of wildfires on the stability and cycling of soil OC. Wildfires can generate a significant quantity of pyrogenic carbon (PyC), produced through the pyrolysis of soil and plant/litter biomass OC under high-temperature and low-oxygen or complete anoxic conditions. Santin et al. [7] highlighted that ~50% of PyC produced during vegetation fires may sequester carbon over centuries, thereby potentially offsetting some of the GHG emissions generated by the fire itself. This is particularly relevant given that wildfires can account for a significant portion of the total carbon emissions in certain regions, with estimates suggesting that they contribute to about 16% of the total PM_{2.5} (fine particulate matter in diameter 2.5 µm or less) emissions in the U.S. [8]. Pyrogenic carbon is believed to be more recalcitrant compared with non-pyrogenic soil OC [9–11]. The overall influence of wildfires on C cycling hinges on several factors including the quantity of GHG emissions generated during combustion, the production of PyC, the physicochemical properties of the PyC, and the impact of wildfires on the biogeochemical cycles of indigenous soil OC [7,8,12].

Furthermore, wildfires significantly disturb the biogeochemical cycles of C, particularly through post-wildfire flooding, which facilitates the migration of C and leaching from terrestrial to aquatic ecosystems [13–15]. Post-wildfire flooding events frequently occur, transporting a substantial amount of OC and other elements to aquatic environments. For example, Abney et al. [16] estimated that after the Gondola fires, approximately 30% of the OC in soils was mobilized and transported through watersheds. The long-term transport of OC after wildfire depends on factors such as soil water repellency and the production of ashes as well as the soil physicochemical properties [17,18]. Wildfires alter soil properties including the OC content, OC and mineral chemical composition, water repellency, and hydrophobicity, influencing runoff and erosion processes [16,19–21]. The influence of wildfire on soil properties is regulated by the fire's severity (defined as the damage of wildfire to the environment) and the characteristics of the burned area [22]. The ashes and PyC generated by wildfires and the high content of hydrophobic OC in post-fire soils can exacerbate erosion and the mobilization of OC [22–24]. A recent review determined that the average OC content of ashes was 204 g/Kg when the high burn severity reduced the OC content in ashes [25]. Physicochemical examination of the ashes uncovered that the higher the combustion temperature, the lighter the color and lower the OC release for the ashes [26]. Consequently, wildfires can elevate the dissolved OC and nutrient loading in aquatic ecosystems of wildfire-impacted watersheds (i.e., lakes, streams, and other waterbodies receiving the runoff), affecting the water quality and treatment requirement for drinking water [27]. There is still controversy regarding how the wildfires impact the mobilization of OC and controlling the physicochemical parameters, given that, in general, the combustion/pyrolysis of biomass and soils not only increases the solubility of OC, but also the content of pyrogenic carbon (PyC), which is less soluble and subject to more complex biogeochemical processes [28,29]. In light of escalating influence of climate change on the intensity and frequency of wildfires, an understanding of the governing factors for the mobility of OC post wildfires is vital for safeguarding both forest catchments and drinking water sources [30–32].

This study focused on OC mobility in the ashes and soils impacted by wildfires in the northern California/Nevada region including the Dixie, Beckwourth Complex, and Caldor fires and the important biogeochemical regulation factors. Major study goals included: (1) measuring the OC mobility in ashes and soils impacted by wildfire; (2) analyzing the impact of the ash and soil physicochemical properties on OC mobility; and (3) identifying

critical factors governing the post-wildfire mobility of OC. Overall, we hypothesized that wildfire may increase the mobility of OC from the soils, which can be predicted based on the physicochemical parameters of the soils and ashes as well as the properties of the wildfire.

2. Materials and Methods

2.1. Study Overview

Water-extractable fractions of OC were used as indicators of OC mobility. For soil particles, the amounts of OC and PyC were measured. Electron paramagnetic resonance (EPR) spectra were analyzed to determine the presence of environmental persistent free radicals (EPFRs). Additionally, the mineral speciation of soils and ashes were determined by X-ray diffraction spectrometry (XRD), and the iron (Fe) oxidation state and speciation were analyzed by synchrotron-based X-ray fluorescence (XRF) and X-ray absorption Near edge structure (XANES) spectroscopy. For the water-extracted OC, in addition to its C content, the aromaticity of OC and redox reactivity were measured. Multiple statistical analyses were used to determine the impact of different physicochemical properties on the mobility of OC.

2.2. Sampling Region and Collection of Soil and Ash Samples

Ash and soil samples were collected from the sites in northern California/Nevada regions, within 2 weeks after the wildfires that occurred in 2021 including the Dixie (DF), Beckwourth Complex (BF2), and Caldor (CF) fires (Figure 1, Table 1) [33,34]. All of these fires occurred mainly in California, close to the borderline with the state of Nevada (Figure 1). A detailed description of all three megafires (Dixie, Beckwourth Complex, and Caldor fires) is provided in the Burned Area Emergency Response (BAER) reports (Supplementary Materials, Figure S1) [33,35,36]. Through this manuscript, BF indicates the site of the Dixie and Beckwourth Complex fires compared with BF2 for the site of the Beckwourth Complex fire only. According to the BEAR reports [33,35,36], all three fires can be defined as medium-to-intense fires. Detailed descriptions of the dominant soils at the Beckwourth, Caldor, and Dixie fires are presented elsewhere [37]. Classification of the soils was performed according to USDA-NRCS using the NRCS Web Soil Survey [38], and the coordinates are given in Table 1. Briefly, the soil is a Meeks gravely loamy coarse sand (Dystric Arenosol), Leptic Phaeozem, Luvic Phaeozem for the sites of the Caldor, Beckwourth, and Dixie fires, respectively. The sampling locations were selected based on the available fire maps and on visual observations of the post-fire landscapes. Visual assessment of the burned areas revealed that for some areas, the burn severity was not homogeneous, and only areas uniformly and fully consumed over an area larger than $\sim 30 \text{ m}^2$ were used for the sampling. The locations with high burn severity were chosen for the sampling, where ground fuels were fully consumed by fire and replicates within a $\sim 5 \text{ m}^2$ area were collected. The samples were collected within two weeks after each individual fire was contained at all three locations, and no precipitation between the fire and sampling time had occurred. More details about the sampling procedure, site, and soil types can be found in previous publications [33,34]. The GPS coordinates of the sampling sites are listed in Table 1. The pictures of all three sampling sites are presented in the Supplementary Materials. Ash samples were collected from the surface (up to 5 cm depth) using a stainless-steel scoop, where litters and soils were avoided based on color and texture. Soil samples were collected from the surface (5–10 cm depth) under the ash layer. As control sites, surface soils (or unburned soil samples) were also collected from the unburned area close (~ 10 – 30 m) to the fire-impacted sites with the same soil type [38]. For each type of sample (ash, unburned, and burned soils), one to two replicates were collected for further analyses. Due to the limited number of samples, for the present study, two replicate samples of each sample

type (ash, unburned and burned soils) were provided. All samples were stored in coolers with ice before being immediately transported to the laboratory, where they were stored at $-18\text{ }^{\circ}\text{C}$. Before analysis, the soils and ashes were freeze-dried at room temperature ($21 \pm 1\text{ }^{\circ}\text{C}$), and large stones and plant root materials were removed. The dry ash and soil particles were ground and sieved through a $200\text{ }\mu\text{m}$ mesh.

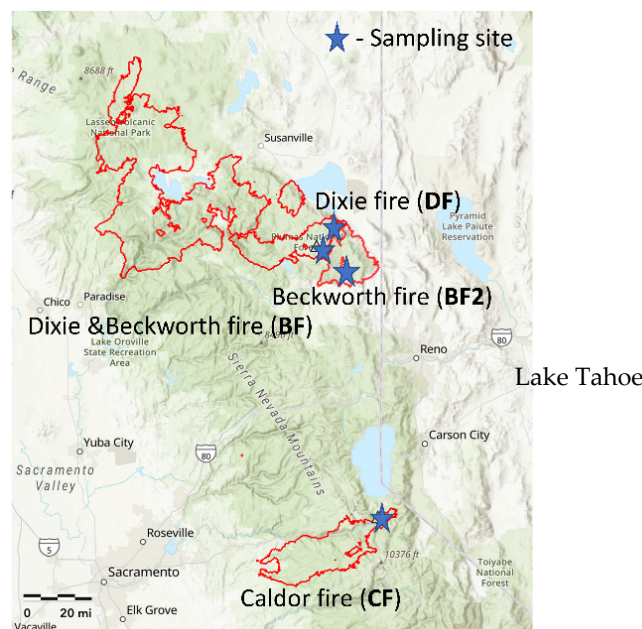


Figure 1. Map of the sampling sites of the wildfire borders in the California Nevada Lake Tahoe region.

Table 1. Summary of the sampling site and fire characteristics [37].

Fire	Burned Area (Acres)	Wildfire Period	Unburned to Low Severity	Medium Severity	High Severity	GPS Coordinates of Sampling Sites
Beckworth Fire (BF2)	105,670	3 July 2021–22 September 2021	44%	53%	3%	39°53'21.1" N 120°12'02.9" W
Caldor Fire (CF)	221,952	14 August 2021–25 October 2021	47%	40%	13%	38°50'37.0" N 120°01'59.8" W
Dixie Fire (DF)	963,309	3 July 2021–22 October 2021	45%	30%	25%	39°58'41.9" N 120°21'24.8" W
Dixie and Beckworth fires (BF)		3 July 2021–22 October 2021				39°56'56.0" N 120°18'18.2" W

2.3. Measurement of Organic Carbon Mobility

The mobile fraction of OC in the ash and soil samples was determined by mixing 10 g (dry weight) of the soil/ash particles with 1 L distilled deionized (DDI) water ($>18\text{ M}\Omega\text{-cm}$). The suspensions were shaken horizontally at 200 rpm for 7 days. Thereafter, the supernatant was filtered with $0.25\text{-}\mu\text{m}$ glass fiber filters and analyzed for dissolved organic carbon (DOC) using a total organic carbon analyzer (Shimadzu TOC-L, Shimadzu Corporation, Kyoto, Japan). Part of the filtered supernatant was used for other analyses. Triplicate analysis were conducted for the mobility of OC.

2.4. Bulk Organic Carbon, Pyrogenic Organic Carbon

The total OC content of the ash and soil samples were determined using a Eurovector elemental analyzer (Eurovector SPA, Milan, Italy). Acetanilide (71.09% C) was used as the calibration standard for OC measurement. For OC measurement, the samples were acidified with 1 mL HCl (1 M)/0.5 g soil/ash and heated at $100\text{ }^{\circ}\text{C}$ for 1 h; the treatment was repeated

until there was no further effervescence upon acid addition. Afterward, the samples were dried and analyzed with the elemental analyzer. Pyrogenic carbon (PyC) was measured following Accardi-Dey and Gschwend [39], where a small aliquot (~500 mg) of the samples was burned under air at 375 °C for 4 h to fully oxidize the labile organic carbon, acidified as described above to remove the inorganic carbon, and then analyzed for the residual C, presumably PyC. Triplicate measurements were made for the content of bulk OC and PyC.

2.5. Specific Surface Area

The specific surface area (SSA) of the ash and soil samples was determined by adsorption/desorption N₂ isotherm measurements using an Autosorb iQ-MP surface area analyzer (Anton Paar USA, Inc. Graz, Austria). Ash samples were degassed at 250 °C for 4 h under vacuum before analysis, while soil samples were degassed at 105 °C for 12 h. The SSA of the samples was calculated using the Brunauer–Emmett–Teller (BET) isotherm method. Duplicate measurements were conducted for the SSA analysis.

2.6. Electron Paramagnetic Resonance

For the analysis of environmental persistent free radicals (EPFRs), measurements were performed directly for the homogenized particle samples using a Bruker EMX-20/2.7 EPR spectrometer (X-band) equipped with dual cavities. The setup parameters included a microwave frequency of 9.785 GHz, power of 6.411 mW, 4 scans, a modulation amplitude of 4.000 G, and a modulation frequency of 100.000 kHz. The center field was set to 3479.060 G, sweep width of 1000.000 G and 200.000 G, time constant of 0.640 ms, conversion time of 20.480 ms, sweep time of 41.943 s, resolution of 2048 points, and receiver gain of 3.99×10^4 , at room temperature. Calibration of field position and spin radical spin concentrations was performed using 2,2-diphenyl-1-picrylhydrazyl (DPPH) as a reference.

2.7. Synchrotron XRF and XANES Spectroscopy

To map the speciation and distribution of iron (Fe), the Beckworth fire (BF) ash, soil, and control soil samples were analyzed at the Stanford Synchrotron Radiation Lightsource (SSRL) beamline 14-3b. 2-3. Beamline 2-3 is a hard X-ray microprobe beamline equipped with a water-cooled double Si (111) monochromator. The monochromator was calibrated to the Fe K-edge using a Fe metal foil (first derivative at 7112 eV). The X-ray beam was focused to a 6x6 μm spot using Sigray axially symmetric focusing optics immediately before the sample. The beamline was equipped with a single channel Hitachi Vortex detector and Quantum Detectors Xspress3 electronics. Data were collected under standard ring conditions of 3 GeV and 500 mA. The freeze-dried and sieved samples were directly mounted onto a silicon wafer that were then loaded onto cassettes within the multi-sample wheel for analysis. The sample wheel position was maintained by Newport stages. The X-ray fluorescence (XRF) mapping for the distribution of iron (Fe), aluminum (Al), silicon (Si), manganese (Mn), and calcium (Ca) was obtained at a resolution of 6–10 μm. For Fe XRF speciation mapping, the images were collected at multiple energies (7114.0, 7115.0, 7122.3, 7127.3, 7133.5 eV). On-the-fly analysis of the multiple energy maps, conducted using the Microanalysis Toolkit [40], assisted in choosing locations for collecting XANES spectra to determine the specific Fe-speciation at individual spots across the sample.

The Microanalysis Toolkit was used to process the XRF maps [40]. The raw fluorescence maps were energy-calibrated and background-corrected using Smak [40]. After applying a Gaussian blur (3-pixel kernel) to smooth the spatial noise, the maps were normalized to eliminate artifacts caused by beam intensity fluctuations. Elemental maps were fit to specific energy levels corresponding to the Fe(II) and Fe(III) oxidation states, facilitating the creation of speciation maps. To generate these maps, we used an iterative fitting algorithm within the Microanalysis Toolkit to account for overlapping fluorescence lines and

matrix effects [40]. Iron XANES spectra were normalized using Athena [41]. Based on a principal component analysis in Athena, up to three major components were required to reconstruct most of the XANES spectra collected across all samples. Therefore, linear combination fitting (LCF) was applied to fit the XANES spectra, with up to 3 standards as determined by principal component analysis, by using a self-built library (based on data shared by Dr. Prachi Joshi, Dr. Beth Tomaszewski, and Dr. Andreas Kappler from the University of Tuebingen (Germany)) composed of the most common soil Fe minerals (i.e., ferrihydrite, goethite, lepidocrocite, carbonate/chlorine/sulfate greenrust, and siderite). Based on the LCF results, the average oxidation state of Fe and fraction of Fe(II)/Fe(III) was calculated. Accounting for the major Fe minerals determined by LCF, XRF mappings at multiple energy levels were also fit to obtain the microscale distribution of Fe(II)/Fe(III).

2.8. XRD

The mineral compositions of the soil and ash samples were also analyzed with a BRUKER APEX II X-ray diffractometer (BRUKER, Billerica, MA, USA), and the major mineral species were identified by comparing the spectra with the crystallography open database [42].

2.9. Redox Reactivity Measurement

The redox reactivity of the mobilized OC was analyzed with a chemical assay developed previously [43,44]. In brief, the mobilized OC (filtrate) of the soil and ash was reduced by *Shewanella putrefaciens* CN32 (10^8 cells/mL, pH 7, 3 mM bicarbonate), using H_2 as the terminal electron donor. The 24-h microbially reduced OC was reacted with Fe(III)-NTA, and the generated Fe(II) was measured by a ferrozine assay and used to calculate the electron donation by the microbially-reduced OC, as a measurement of the electron acceptance capacity of the OC. In association with the redox reactivity measurement for the mobilized OC, the filtrate was also analyzed for the UV-absorption spectra, and SUVA₂₅₄ (specific UV absorption at 254 nm normalized by the concentration of OC) was calculated as the indicator for the aromaticity of OC.

2.10. Statistical Analysis

Statistical analysis (e.g., Pearson correlation analysis, *t*-test and others) was undertaken with SPSS Statistics 29 (v29.0.1.1) (IBM, SPSS Inc. New York, NY, USA). To evaluate the effects of the sample type (ash, soil, control) and site (BF, DF, CF, BF2) on the measured variables (e.g., surface area, OC mobility), a two-way analysis of variance (ANOVA) was conducted. Post hoc comparisons were performed using Tukey's honest significant difference (HSD) test to identify pairwise differences between groups with a statistical significance threshold of $p < 0.05$.

3. Results

3.1. Mobility of OC in Ashes and Soils

The bulk OC content in the ashes ranged from 9.2 ± 0.38 to 57.3 ± 5.4 mg/g while the control soil OC content ranged from 4.3 ± 0.25 to 24.4 ± 4.6 mg/g. Bulk OC content in the soil under ashes ranged from 9.5 ± 1.8 to 25.7 ± 2.1 mg/g (Figure 2). The OC contents in BF-A, BF-S, CF-A, BF2-A, and BF2-S were significantly higher than the corresponding control soils (*t*-test, $p < 0.05$).

After shaking with DDI water for 7 days, the fraction of mobile OC was as high as 0.07. The fraction of mobile carbon ranged from 0.0093 ± 0.0042 to 0.029 ± 0.010 for ashes, from 0.025 ± 0.015 to 0.070 ± 0.033 for soil under ashes, and from 0.010 ± 0.0031 to 0.066 ± 0.014 for soils from the control sites (Figure 3). The mobile fraction in ashes was 69.8% lower than the control soils for the Beckworth fire ($p < 0.05$). The mobile fraction of OC in the soil under

ash was higher than the control soils for DF and CF ($p < 0.05$). The mobile OC content (bulk OC content \times mobile fraction) ranged from 0.129 ± 0.010 mg OC/g to 1.85 ± 0.096 mg/g. The mobile OC in the ashes (0.266 ± 0.0038 mg/g to 0.743 ± 0.029 mg/g) and soil under ashes (0.547 ± 0.018 mg/g to 1.85 ± 0.096 mg/g) was both higher than that in the control soils (0.129 ± 0.010 mg/g to 0.275 ± 0.015 mg/g), while the difference was significant for BF-S, DF-S, CF-S, BF2-A, and BF2-S ($p < 0.05$). Specifically, the mobile OC in ashes was 1.05–3.53 times the values for the control soils, while the mobile OC in the soil under ashes was 1.94–6.74 times that of the control.

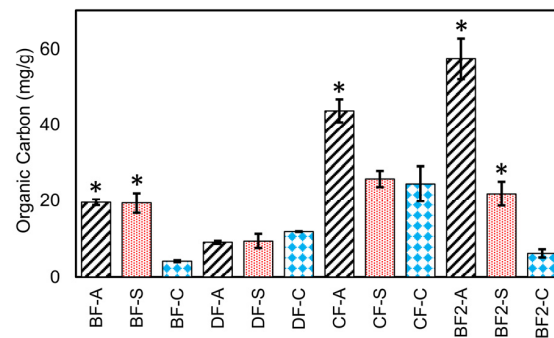


Figure 2. Bulk organic carbon (OC) content for ashes (-A), soil under ash (-S), and control soils (-C) for different sites. BF indicates the site of the Dixie and Beckworth fire, DF indicates the site of the Dixie fire, CF indicates the site of the Caldor fire, and BF2 indicates the site of the Beckworth Complex fire. The labels are the same for all figures in this manuscript. Error bars represent the standard deviation for the triplicate measurements. Asterisks indicate samples with a significant difference in comparison with the control soils ($p < 0.05$).

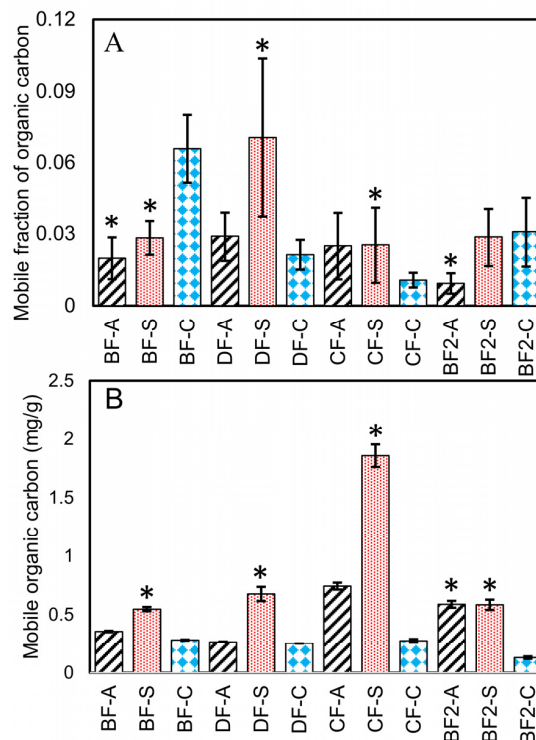


Figure 3. Mobile fraction (unitless) of organic carbon (A) and mobile organic carbon (B) in the ashes (-A), soil under ash (-S), and control soils (-C) for the different sites. Error bars represent the standard deviation for the triplicate measurements. Asterisks indicate samples with a significant difference in comparison with the control soils ($p < 0.05$).

3.2. Physicochemical Properties of Particles of Ashes and Soils

The specific surface area of all samples ranged from 3.80 ± 0.370 to 18.9 ± 5.03 m²/g, while the desorption displayed hysteresis (Figure 4). The specific surface area of ashes was smaller than the control soils for BF, but higher for CF and BF2; the soil under ash had a smaller specific surface area than that of the control soils for BF and CF, but was higher for DF and BF2. Considering the standard deviation, the surface area of ash was significantly higher than that of the control for CF ($p < 0.05$).

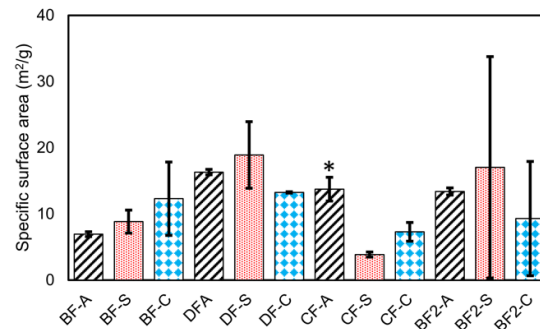


Figure 4. Specific surface area (m²/g) for ashes (-A), soil under ash (-S), and control soils (-C). Error bars represent the standard deviation for the triplicate measurements. Asterisks indicate samples with a significant difference in comparison with the control soils ($p < 0.05$).

As an important chemical property of the soil OC, especially in terms of the impact of wildfires, the PyC content ranged from 0.83 ± 0.043 to 13.7 ± 0.61 mg/g (Figure 5), and the fraction of PyC in the OC range was 6.7–84.2%. The content of PyC was higher in the ash than the background soils, except for CF.

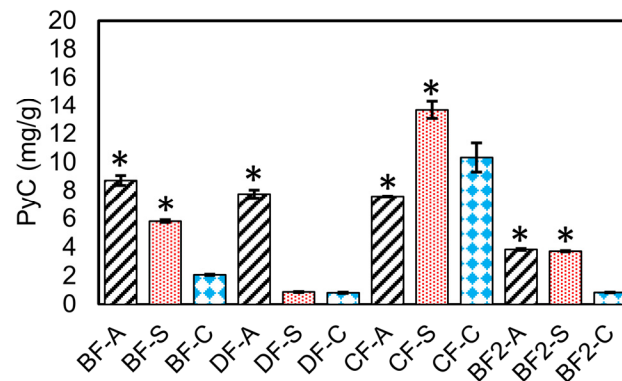


Figure 5. Content of pyrogenic carbon (PyC) (mg/g) in the ash (-A), soil under ash (-S), and control soil samples (-C). Error bars represent the standard deviation for the triplicate measurements. Asterisks indicate samples with a significant difference in comparison with the control soils ($p < 0.05$).

Electron paramagnetic resonance (EPR) spectra were used to analyze the environmentally persistent free radicals (EPFRs). The signals were captured for the ashes of DF and CF with an intensity of 2.0×10^{18} and 6.9×10^{17} spins/g, corresponding to the high content of PyC in DF and CF ash (9.5 and 36 mg/g, respectively) (Figure 6). The g value of the EPFR was 2.00305 and 2.00295 for DF and CF ash, respectively, suggesting a carbon-centered radical adjacent to an oxygen atom and carbon-centered radical. A strong radical signal (1.23×10^{17} spins/gram) with a g -value of 2.0029 was detected for the CF soil under ash, consistent with its high content PyC of 21.9 mg/g.

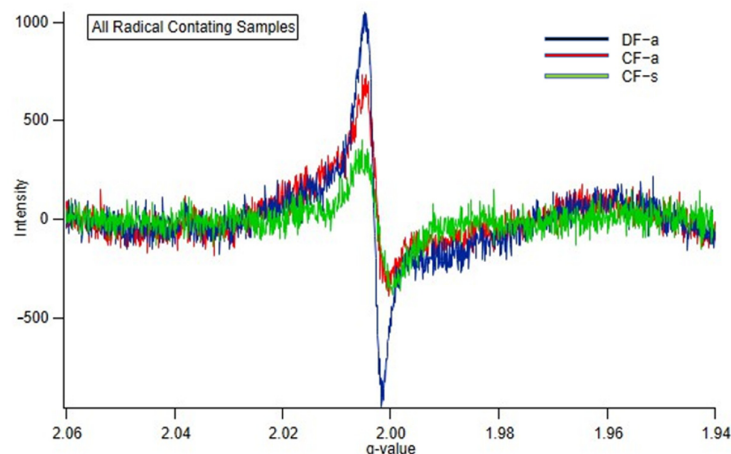


Figure 6. Electron paramagnetic resonance (EPR) spectra for ashes from the Dixie fire (DF-a) and Caldor fire (CF-a) and soil under ash from the Caldor fire (CF-s).

XRD spectra analysis determined that the major minerals were calcite and quartz in the ashes, while the soil under ash and background soils were dominated by aluminosilicates (Figure 7). The XRD peak ($2\theta = 26.7^\circ$) corresponding to graphite was detected in DF-A, consistent with the presence of PyC in ashes and its relatively high content.

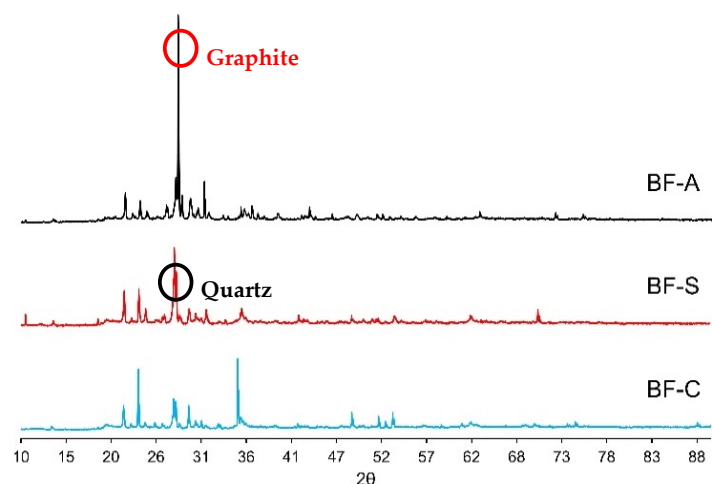


Figure 7. Example XRD results for the ash, soil under ash, and control soil from BF sites.

In addition to the XRD analysis for major minerals, XRF maps for the microscale distribution of major elements including silicon (Si), iron (Fe), calcium (Ca), magnesium (Mg), and manganese (Mn) were also collected for ashes, soil under ash, and soils from BF (Figure 8). There was a correlation between the XRF signal for Fe and Si, implying that Fe might be incorporated into Si-bearing minerals such as clays, as detected by XRD.

X-ray absorption near edge structure (XANES) spectra were collected for hot spots of Fe for the BF ashes particles, soil under ash, and background soils (Figure 8). The XRF spectra of the ash ($N = 26$), soil under ash ($N = 16$), and control soils ($N = 12$) were fitted through linear combination fitting (LCF) using standards including most of the common Fe minerals in soils (i.e., ferrihydrite, goethite, lepidocrocite, carbonate/chlorine/sulfate greenrust, and siderite), with an average r -factor of 0.037 ± 0.017 , 0.102 ± 0.087 , and 0.036 ± 0.028 for the ash, soil under ash, and control soils, respectively (Figure 9). Based on the fitting, the ashes were composed of 60.9% of Fe(II) and 39.1% of Fe(III); similarly to the ashes, the control soils were composed of 64.3% Fe(II) and 35.7% Fe(III). In contrast, the

soil under ashes were substantially different in terms of the composition of Fe(II)/Fe(III) ratio, with 1.98% iron occurring as Fe(II) and iron occurring in 98.0% as Fe(III) (Figure 10).

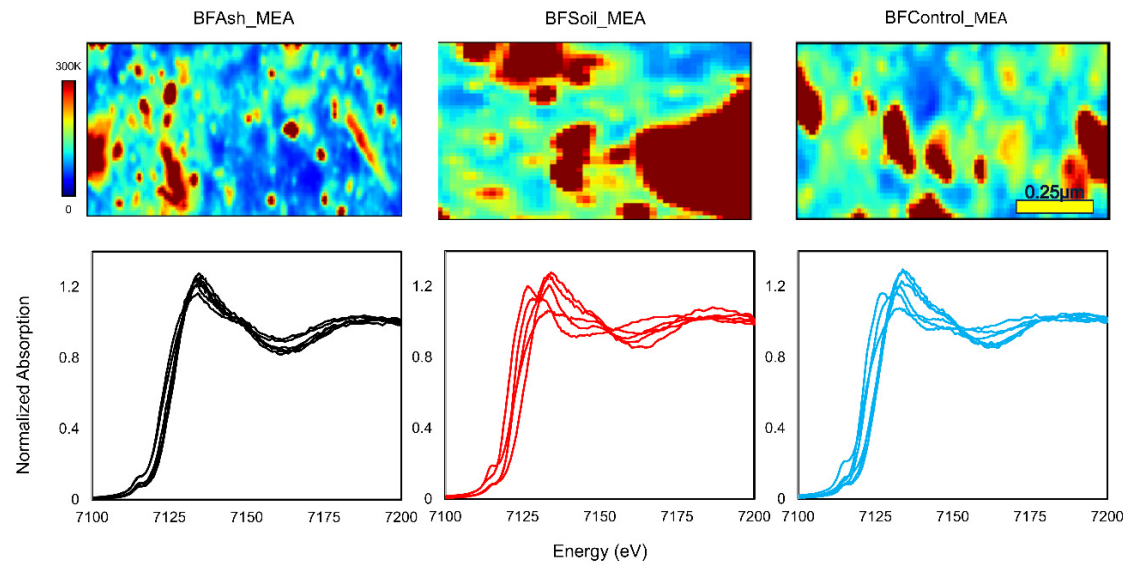


Figure 8. X-ray fluorescence (XRF) map of iron (Fe) distribution in particles (**top row**) for the control soils, soil under ash, and ashes from the Beckworth fire (BF) sites and the Fe K-edge XANES spectra collected (**bottom row**).

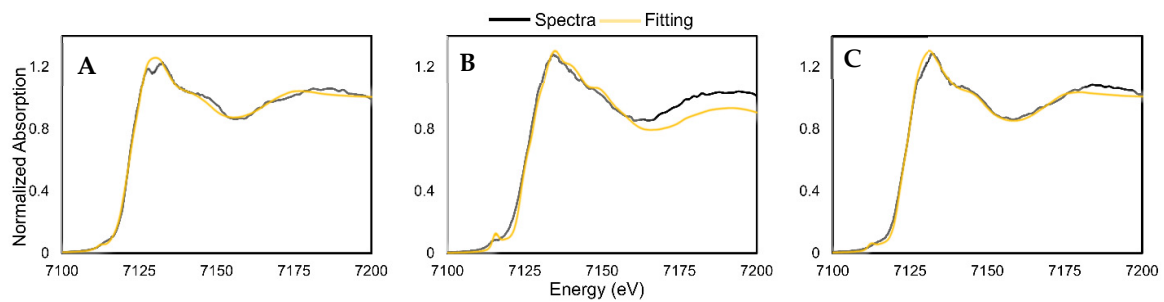


Figure 9. Representative linear combination fitting results for the BF ash (A), soil under ash (B), and control soils (C).

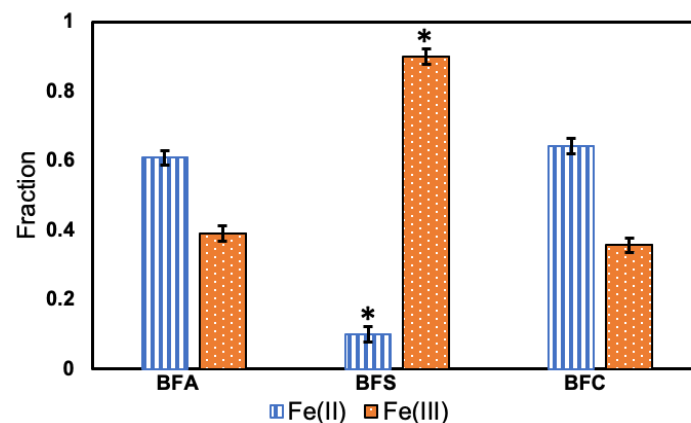


Figure 10. Linear combination fitting-based fraction of the Fe(II) and Fe(III) relative abundances in BF-A (ash), BF-S (soil under ash), and BF-C (control soils). Asterisks indicate samples with a significant difference in comparison with the control soils ($p < 0.05$).

Based on the XANES collected for the samples, the multi-energy XRF collected for the ashes, soil under ash, and reference soils were fitted to map the Fe(II) and Fe(III) on the BF particles (Figure 11).

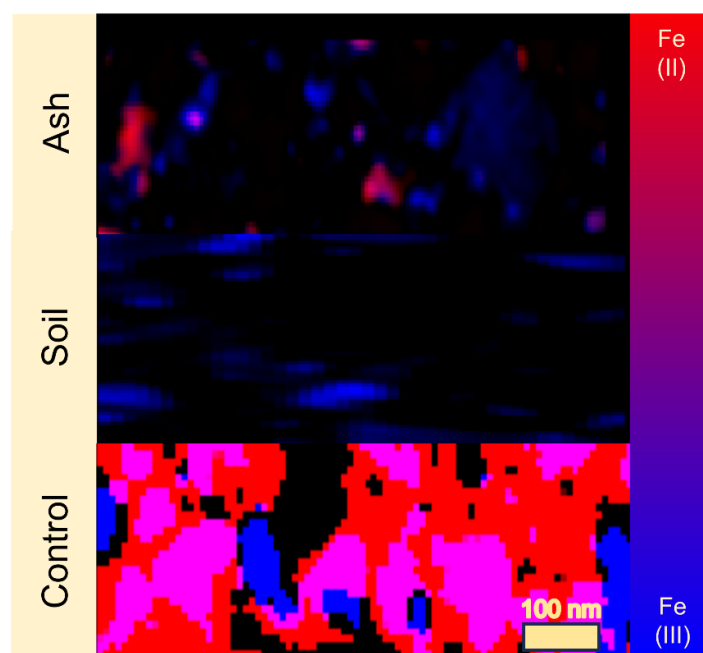


Figure 11. Bi-color microscale distribution of Fe(II)/Fe(III) in the ash, soil under ash, and control soils at the Beckworth fire site.

3.3. Physicochemical Properties of Mobile OC

3.3.1. UV

UV spectra were collected for the ashes, soil under ash, and control soils, with feature absorption at 254 nm for the ashes indicating the contribution of aromatic carbon. Quantitatively, the $SUVA_{254}$ -based fraction of aromatic carbon in dissolved OC ranged from 12.8–25.4%, 24.5–37.0%, and 20.2–28.6% for the ashes, soil under ash, and control soils, respectively. The fraction of aromatic carbon in dissolved OC was lower for ashes compared with the control soils, except for BF.

3.3.2. Redox Reactivity

The electron acceptance capacity was detected for the samples of ashes, soil under ash, and control soils, with values of 0.000 ± 0.001 to 0.558 ± 0.000 , 0.000 ± 0.002 to 0.224 ± 0.241 , and 0.000 ± 0.010 to 0.930 ± 0.028 mmol e⁻/mL, respectively. Although the chemical nature of redox-reactive organic carbon is not fully understood, assuming the key electron-mediated center as quinone/semiquinones, the redox-reactive organic carbon was calculated as $0.157 \pm 0.001\%$, $0.197 \pm 0.001\%$, and $0.163 \pm 0.000\%$ of the total dissolved organic carbon for the ash, soil under ash, and control soil, respectively.

4. Discussion

4.1. Impact of Chemical vs. Physical Properties of Ashes and Soils on the Mobility of OC

Among all of the physicochemical parameters measured in this study, the only significant correlation observed was the inverse correlation between the mobile fraction of OC and the OC content (Kendall coefficient $r = -0.485$, $p = 0.028$), although it was noted that these two factors were not completely independent of each other. These analyses indicate that the mobile fraction of OC may not be governed by a single physicochemical property of the ashes and/or the wildfire-impacted soils. It is widely observed that the specific surface area

can be important for the release of OC as well as other elements due to surface functionality dynamics [45]. Thermal reactions and alteration in the aggregation of soil particles during wildfires can change the specific surface area of soil particles, although no consistent trend was observed in this work. Contrasting observations in the literature regarding the impact of wildfire on the soil porosity and specific surface areas were made as follows: wildfire can lead to thermal expansion of the soil organic matter and minerals, decreasing the bulk density but increasing the surface area and porosity; in contrast, wildfires can also destroy the structures of soil organic matter, leading to their collapse and reducing the specific surface area [46]. While no single factor strongly correlated with OC mobility, the mobile OC can be estimated using a linear regression incorporating multiple variables measured in this study (Equation (1), $p = 0.1$) (Figure 12).

$$OC_{mobile} = 0.013 SA + 0.015 OC + \frac{0.492PyC}{OC} - 0.035 SUVA_{254} + 0.009 \quad (1)$$

where OC_{mobile} is the mobile OC, SA is the specific surface area, PyC is the bulk content of pyrogenic carbon, OC is the bulk content of organic carbon, and $SUVA_{254}$ is the specific UV absorption at 254 nm normalized by the dissolved OC content. While this empirical regression should not be overinterpreted, it indicates the positive contribution of specific surface area and pyrogenic carbon.

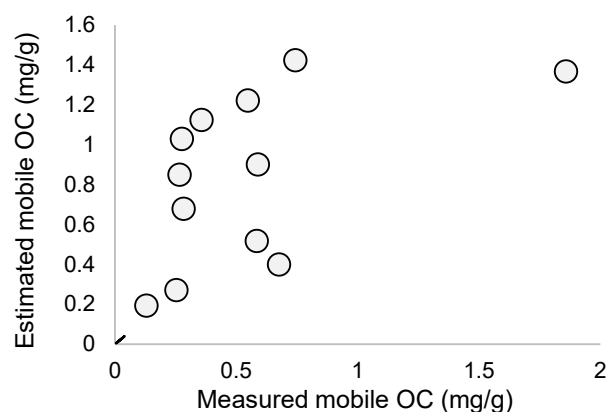


Figure 12. Relationship between the measured mobile organic carbon (OC) and predicted values based on the empirical linear regression (Equation (1)).

4.2. Role of Redox Reactions in the OC Mobility

Redox reactivities of the ashes and soils were demonstrated through multiple analyses. EPR analysis determined the presence of carbon-centered radicals and carbon-centered radicals adjacent to the oxygen atom in the ashes of DF and CF as well as in the soil under ash of CF. Sigmund [47] reported EPR signals with intensities ranging from concentrations of 2.4×10^{18} spins/g to 1.5×10^{19} spins/g for charcoals generated from a range of fires. Such EPFRs are important for redox reactions occurring in soil environments; some of the EPFRs can be contributed by semiquinones, one of the most important electron shuttles, as demonstrated by previous studies [48–50]. Lokesh et al. [51] determined a semi-benzoquinone generated by the reaction between hydrobenzoquinone and $FeCl_3$ with a g value of $g = 2.031$ [51]. The strong EPR signals of these samples were consistent with their high content of pyrogenic carbon.

XANES-XRF analysis showed a clear difference in the oxidation state of Fe in the soil under ashes (with 1.98% of iron as Fe(II)) compared to the ash and background soils (with 35.7–64.3% of iron as Fe(II)). Our data suggest that under heating, Fe(II) minerals in the soils were thermal-oxidized to Fe(III), with the Fe speciation in ash reflecting the mixture of Fe

speciation in burned biomass together with the Fe in soil after burning. The XANES fitting indicates that the dominant Fe minerals in soil under ash were most likely ferrihydrite and lepidocrocite/goethite compared with more greenrust in the control soils and ashes. The XANES results, fitting to multi-wavelength XRF, also showed the distribution of Fe(III) among particles, which correlates and co-locates with silicon, providing strong evidence of potential microscale hot spots of mobile organic carbon.

Soil is not a good conductor of heat, so a large gradient is needed for fire to affect the soil under ash layers [52]. With 2021 being a drought year, it is most likely that the soils experienced a step heat gradient, with the rapid vaporization of moisture taking place. For the limited sites available at BF—ashes, soil under ashes, and control soils—an inverse relationship between OC mobility and Fe(II) (Kendall correlation coefficient = -1) was observed, where the lower fraction of Fe(II), the higher mobility of OC. The thermal oxidation of Fe(II) in soils has been associated with arsenic mobilization [53]. Such thermal oxidation of Fe(II) and the associated mobilization of Fe-bound OC can be promoted by the presence of PyC, which can act as an electron shuttle to facilitate the oxidation of Fe(II) [54–56]. Part of the OC mobilized to the solution phase also showed redox reactivity, with the electron acceptance capacity measured to be between 0.000 ± 0.001 and 0.937 ± 0.028 mol e^- /L, potentially contributed by quinones, as suggested in previous studies [51]. The aromatic fraction of the mobilized OC, determined by $SUVA_{254}$, ranged from 12.8 to 37.0%, which also correlated with the redox reactivity of the bulk OC.

4.3. Influences of Wildfire Properties

The physicochemical properties of ashes and soil under ashes can be significantly influenced by wildfire characteristics including severity, burning area, and surface vegetation. The severity of wildfires studied for the region ranged from 47 to 50% for low to middle severity, and 2–13% burned at high severity. Semi-quantitatively, the more severe a wildfire is, the more mobile organic carbon is yielded. Field measurements and laboratory studies have shown that the more severe the wildfire is, then the higher temperatures result in the ambient air and on soil surfaces [57]. Overall, fire severity dictates temperature and oxygen present, the concentration of which, in turn, influences the properties of the wildfire-derived ashes and impacted soils.

4.4. Implication on Watershed Functions

The carbon storage of the soil in the Lake Tahoe region is estimated to be $\sim 10,000$ g/m² [58]. Additionally, inflow from Angora Creek into Lake Tahoe has an average concentration of 0.5 μ g/L of PyC, which represents $\sim 1\%$ of Lake Tahoe run-off, equating to ~ 1.6 kg for the winter [59]. Interestingly, these PyC concentrations were connected to the episodic events of fires and snowmelt, and suggest that lake concentrations resulting from fire can result from atmospheric deposition [59]. Our analysis indicates that the carbon content in the ash layers approximately 1 cm thick at the BF, DF, and CF sites is estimated at 100, 396, and 332 g/m², respectively, assuming an ash density of 400 kg/m³ [9]. In comparison, the surface 1-cm soil at these sites contained 315, 144, and 792 g C/m², respectively, assuming a density of 1440 kg/m³ [60]. Furthermore, the estimated mobile carbon from this pool was 2, 10.7, and 3.3 g/m², respectively, in comparison to 2–3 g/m² from the corresponding control sites. Considering the burning area of 3.9×10^9 for DF and BF and 8.8×10^8 m² for CF, wildfires could potentially increase the mobility of up to between 2.8×10^{10} and 6.3×10^9 g of carbon, reflecting an increase of 7 g/m² in mobile carbon. For CF, the mobilization of OC into Lake Tahoe could potentially contribute to an increase in dissolved OC concentration in the lake. Specifically, if the OC from the surface 1 cm of ash is mobilized, this could lead to a dissolved

OC increase of 0.04 mg/L in Lake Tahoe ($150.7 \times 10^9 \text{ m}^3$) compared with around 0.3 mg/L OC for the current level [61].

5. Conclusions

This study highlights the intricate interplay of factors influencing the properties of wildfire-derived ashes and the governing factors for fire-induced OC mobilization. Our research demonstrates that up to 7.0% of the OC in wildfire-derived ashes or impacted soils was labile during water extraction, representing the portion of carbon that can be mobilized and transported following wildfires. The mobile fraction of OC in the ashes was substantially higher than that in the control soils for the Dixie and Caldor fires, whereas it was lower for the Beckworth fire. Nonetheless, across all sites, the content of mobile OC was significantly increased by the wildfires compared with the control soils. While no single physicochemical parameter of the ashes or soils showed a strong bivariate correlation with the mobility of OC, the mobile OC could be estimated using an empirical multivariate linear regression, indicating that the mobile OC was regulated by multiple biogeochemical processes. XRF-XANES analysis provided compelling evidence for the thermal oxidation of Fe(II) in the soil under ashes, which correlated with the mobility of OC. This indicates that the thermal oxidation of ferrous minerals can be promoted by the presence of redox-reactive PyCs and EPFRs, which can lead to the mobilization of OC bound with Fe minerals. The enhanced mobility of wildfire-derived mobile OC can lead to the substantial transport of OC to aquatic ecosystems, potentially causing harmful effects. These findings underscore the importance of understanding the processes governing OC mobility in wildfire-impacted environments, which is crucial for effective wildfire management and mitigation strategies aimed at protecting watersheds.

Supplementary Materials: The following supporting information can be downloaded at: <https://www.mdpi.com/article/10.3390/soilsystems9010011/s1>, Figure S1 Typical vegetation and soil surface conditions at fire sites.

Author Contributions: Conceptualization, T.N. and Y.Y.; Methodology, Y.Y.; Software, T.N.; Validation, T.N. and Y.Y.; Formal analysis, T.N.; Investigation, T.N., S.L., A.S., A.T. and J.C.; Resources, T.N., Y.R., V.S. and Y.Y.; Data curation, T.N., M.L.L., Q.Z., S.R.P., P.S.V., J.A.R. and R.L.C.; Writing—original draft preparation, T.N.; Writing—review and editing, All authors; Visualization, T.N.; Supervision, Y.Y.; Project administration, Y.Y.; Funding acquisition, T.N. and Y.Y. All authors have read and agreed to the published version of the manuscript.

Funding: This work was also partially supported by NSF No. 2108270 and No. 2148056, along with the National Institute of Environmental Health Science (NIEHS) Superfund Research Program (award #P42 ES013648) as well as the NIFA Nevada Tribal Students grant. This research was supported by the Stanford Synchrotron Radiation Lightsource (SSRL) user proposal S-XV-ST-5898. The use of the SSRL, SLAC National Accelerator Laboratory, was supported by the U.S. Department of Energy (DOE), Office of Science, Office of Basic Energy Sciences under Contract No. DE-AC02-76SF00515. The SSRL Structural Molecular Biology Program is supported by the DOE Office of Biological and Environmental Research, and by the National Institutes of Health, National Institute of General Medical Sciences (P30GM133894). The contents of this publication are solely the responsibility of the authors and do not necessarily represent the official views of the NIGMS or NIH.

Institutional Review Board Statement: Not applicable.

Informed Consent Statement: Not applicable.

Data Availability Statement: The original contributions presented in this study are included in the article and Supplementary Materials. Further inquiries can be directed to the corresponding author.

Acknowledgments: Travis Numan thanks the support by the University of Nevada College of Engineering Indigenous Engineering Fellowship. Yu Yang acknowledges the support by the Alexander von Humboldt Research Fellowship. We also thank Prachi Joshi, Beth Tomaszewski, and Andreas Kappler from the University of Tuebingen (Germany) for the XANES reference library, and Prachi Joshi for the helpful discussions.

Conflicts of Interest: The authors declare no conflict of interest.

References

1. Westerling, A.L.; Hidalgo, H.G.; Cayan, D.R.; Swetnam, T.W. Warming and earlier spring increase western US forest wildfire activity. *Science* **2006**, *313*, 940–943. [[CrossRef](#)] [[PubMed](#)]
2. Uzun, H.; Zhang, W.B.; Olivares, C.I.; Erdem, C.U.; Coates, T.A.; Karanfil, T.; Chow, A.T. Effect of prescribed fires on the export of dissolved organic matter, precursors of disinfection by-products, and water treatability. *Water Res.* **2020**, *187*, 116385. [[CrossRef](#)]
3. Abatzoglou, J.T.; Williams, A.P.; Boschetti, L.; Zubkova, M.; Kolden, C.A. Global patterns of interannual climate-fire relationships. *Glob. Change Biol.* **2018**, *24*, 5164–5175. [[CrossRef](#)] [[PubMed](#)]
4. Williams, A.P.; Livneh, B.; McKinnon, K.A.; Hansen, W.D.; Mankin, J.S.; Cook, B.I.; Smerdon, J.E.; Varuolo-Clarke, A.M.; Bjarke, N.R.; Juang, C.S.; et al. Growing impact of wildfire on western US water supply. *Proc. Natl. Acad. Sci. USA* **2022**, *119*, e2114069119. [[CrossRef](#)] [[PubMed](#)]
5. Lasslop, G.; Coppola, A.I.; Voulgarakis, A.; Yue, C.; Veraverbeke, S. Influence of Fire on the Carbon Cycle and Climate. *Curr. Clim. Change Rep.* **2019**, *5*, 112–123. [[CrossRef](#)]
6. Jones, M.W.; Santín, C.; van der Werf, G.R.; Doerr, S.H. Global fire emissions buffered by the production of pyrogenic carbon. *Nat. Geosci.* **2019**, *12*, 742–747. [[CrossRef](#)]
7. Santín, C.; Doerr, S.H.; Kane, E.S.; Masiello, C.A.; Ohlson, M.; De La Rosa, J.M.; Preston, C.M.; Dittmar, T. Towards a global assessment of pyrogenic carbon from vegetation fires. *Glob. Change Biol.* **2016**, *22*, 76–91. [[CrossRef](#)]
8. Prichard, S.J.; O'Neill, S.M.; Eagle, P.; Andreu, A.G.; Drye, B.; Dubowy, J.; Urbanski, S.; Strand, T.M. Wildland fire emission factors in North America: Synthesis of existing data, measurement needs and management applications. *Int. J. Wildland Fire* **2020**, *29*, 132. [[CrossRef](#)]
9. Santín, C.; Doerr, S.H.; Preston, C.M.; González-Rodríguez, G. Pyrogenic organic matter production from wildfires: A missing sink in the global carbon cycle. *Glob. Change Biol.* **2015**, *21*, 1621–1633. [[CrossRef](#)] [[PubMed](#)]
10. Bird, M.I.; Wynn, J.G.; Saiz, G.; Wurster, C.M.; McBeath, A. The Pyrogenic Carbon Cycle. *Annu. Rev. Earth Planet. Sci.* **2015**, *43*, 273–298. [[CrossRef](#)]
11. Abney, R.B.; Berhe, A.A. Pyrogenic Carbon Erosion: Implications for Stock and Persistence of Pyrogenic Carbon in Soil. *Front. Earth Sci.* **2018**, *6*, 26. [[CrossRef](#)]
12. Stephens, E.Z.; Homyak, P.M. Post-fire soil emissions of nitric oxide (NO) and nitrous oxide (N₂O) across global ecosystems: A review. *Biogeochemistry* **2023**, *165*, 291–309. [[CrossRef](#)]
13. Santos, F.; Wymore, A.S.; Jackson, B.K.; Sullivan, S.M.P.; McDowell, W.H.; Berhe, A.A. Fire severity, time since fire, and site-level characteristics influence streamwater chemistry at baseflow conditions in catchments of the Sierra Nevada, California, USA. *Fire Ecol.* **2019**, *15*, 3. [[CrossRef](#)]
14. Thuile Bistarelli, L.; Poyntner, C.; Santín, C.; Doerr, S.H.; Talluto, M.V.; Singer, G.; Sigmund, G. Wildfire-Derived Pyrogenic Carbon Modulates Riverine Organic Matter and Biofilm Enzyme Activities in an In Situ Flume Experiment. *ACS EST Water* **2021**, *1*, 1648–1656. [[CrossRef](#)] [[PubMed](#)]
15. Hutchins, R.H.S.; Tank, S.E.; Olefeldt, D.; Quinton, W.L.; Spence, C.; Dion, N.; Mengistu, S.G. Influence of Wildfire on Downstream Transport of Dissolved Carbon, Nutrients, and Mercury in the Permafrost Zone of Boreal Western Canada. *J. Geophys. Res. Biogeosciences* **2023**, *128*, e2023JG007602. [[CrossRef](#)]
16. Abney, R.B.; Sanderman, J.; Johnson, D.; Fogel, M.L.; Berhe, A.A. Post-wildfire Erosion in Mountainous Terrain Leads to Rapid and Major Redistribution of Soil Organic Carbon. *Front. Earth Sci.* **2017**, *5*, 99. [[CrossRef](#)]
17. Rhoades, C.C.; Nunes, J.P.; Silins, U.; Doerr, S.H. The influence of wildfire on water quality and watershed processes: New insights and remaining challenges. *Int. J. Wildland Fire* **2019**, *28*, 721–725. [[CrossRef](#)]
18. Pellegrini, A.F.A.; Reich, P.B.; Hobbie, S.E.; Coetsee, C.; Wigley, B.; February, E.; Georgiou, K.; Terrer, C.; Brookshire, E.N.J.; Ahlström, A.; et al. Soil carbon storage capacity of drylands under altered fire regimes. *Nat. Clim. Chang.* **2023**, *13*, 1089–1094. [[CrossRef](#)]
19. Staley, D.M.; Kean, J.W.; Cannon, S.H.; Schmidt, K.M.; Laber, J.L. Objective definition of rainfall intensity-duration thresholds for the initiation of post-fire debris flows in Southern California. *Landslides* **2013**, *10*, 547–562. [[CrossRef](#)]
20. Ebel, B.A. Upper limits for post-wildfire floods and distinction from debris flows. *Sci. Adv.* **2024**, *10*, eadk5713. [[CrossRef](#)] [[PubMed](#)]

21. Wehner, M.F.; Arnold, J.R.; Knutson, T.; Kunkel, K.E.; LeGrande, A.N. Chapter 8: Droughts, Floods, and Wildfires. In *Climate Science Special Report: Fourth National Climate Assessment*; U.S. Global Change Research Program: Washington, DC, USA, 2017; Volume I. [CrossRef]
22. Certini, G. Effects of fire on properties of forest soils: A review. *Oecologia* **2005**, *143*, 1–10. [CrossRef] [PubMed]
23. Knicker, H. How does fire affect the nature and stability of soil organic nitrogen and carbon? A review. *Biogeochemistry* **2007**, *85*, 91–118. [CrossRef]
24. Neary, D.G. NForest Soil Disturbance: Implications of Factors Contributing to the Wildland Fire Nexus. *Soil Sci. Soc. Am. J.* **2019**, *83*, S228–S243. [CrossRef]
25. Sánchez-García, C.; Santín, C.; Neris, J.; Sigmund, G.; Otero, X.L.; Manley, J.; González-Rodríguez, G.; Belcher, C.M.; Cerdà, A.; Marcotte, A.L.; et al. Chemical characteristics of wildfire ash across the globe and their environmental and socio-economic implications. *Environ. Int.* **2023**, *178*, 108065. [CrossRef] [PubMed]
26. Rodela, M.H.; Chowdhury, I.; Hohner, A.K. Emerging investigator series: Physicochemical properties of wildfire ash and implications for particle stability in surface waters. *Environ. Sci. Process. Impacts* **2022**, *24*, 2129–2139. [CrossRef]
27. Bladon, K.D.; Emelko, M.B.; Silins, U.; Stone, M. Wildfire and the Future of Water Supply. *Environ. Sci. Technol.* **2014**, *48*, 8936–8943. [CrossRef] [PubMed]
28. Wagner, S.; Ding, Y.; Jaffe, R. A New Perspective on the Apparent Solubility of Dissolved Black Carbon. *Front. Earth Sci.* **2017**, *5*, 16. [CrossRef]
29. Sánchez, R.A.; Meixner, T.; Roy, T.; Ferré, P.T.; Whitaker, M.; Chorover, J. Physical and biogeochemical drivers of solute mobilization and flux through the critical zone after wildfire. *Front. Water* **2023**, *5*, 1148298. [CrossRef]
30. Abatzoglou, J.T.; Williams, A.P. Impact of anthropogenic climate change on wildfire across western US forests. *Proc. Natl. Acad. Sci. USA* **2016**, *113*, 11770–11775. [CrossRef] [PubMed]
31. Bachelet, D.; Lenihan, J.M.; Neilson, R.P. The importance of climate change for future wildfire scenarios in the western United States. In *Regional Impacts of Climate Change: Four Case Studies in the United States*; Pew Center on Global Climate Change: Arlington, VA, USA, 2007.
32. Cassell, B.A.; Scheller, R.M.; Lucash, M.S.; Hurteau, M.D.; Loudermilk, E.L. Widespread severe wildfires under climate change lead to increased forest homogeneity in dry mixed-conifer forests. *Ecosphere* **2019**, *10*, e02934. [CrossRef]
33. U.S. Department of Agriculture Forest Service. Beckwourth Complex Post-Fire BAER Assessment Report. Available online: <https://www.fire.ca.gov/incidents/2021/7/4/beckwourth-complex> (accessed on 25 November 2022).
34. Institute, C.B. California Fire Perimeters (1898–2020). Available online: <https://databasin.org/datasets/bf8db57ee6e0420c8ecce3c6395aceeb/> (accessed on 26 November 2022).
35. Ellsworth, T.; Stamer, M. *Caldor Fire Burned Area Emergency Response (BAER) Assessment Report Summary*; U.S. Department of Agriculture Forest Service: Washington, DC, USA, 2021; pp. 4–16.
36. U.S. Department of Agriculture Forest Service. Dixie Post-Fire BAER Assessment Report. Available online: <https://www.fire.ca.gov/incidents/2021/7/13/dixie-fire/> (accessed on 25 November 2022).
37. Samburova, V.; Schneider, E.; Rüger, C.P.; Inouye, S.; Sion, B.; Axelrod, K.; Bahdanovich, P.; Friederici, L.; Raefoy, Y.; Berli, M.; et al. Modification of Soil Hydroscopic and Chemical Properties Caused by Four Recent California, USA Megafires. *Fire* **2023**, *6*, 186. [CrossRef]
38. U.S. Department of Agriculture Forest Service. Available online: <https://www.fs.usda.gov/detail/lpnf/home/?cid=fseprd570093> (accessed on 17 January 2025).
39. Accardi-Dey, A.; Gschwend, P.M. Assessing the Combined Roles of Natural Organic Matter and Black Carbon as Sorbents in Sediments. *Environ. Sci. Technol.* **2002**, *36*, 21–29. [CrossRef] [PubMed]
40. Webb, M.S.; McNulty, I.; Eyberger, C.; Lai, B. The MicroAnalysis Toolkit: X-ray Fluorescence Image Processing Software. *AIP Conf. Proc.* **2011**, *1365*, 196–199. [CrossRef]
41. Ravel, B.; Newville, M. ATHENA, ARTEMIS, HEPHAESTUS: Data analysis for X-ray absorption spectroscopy using IFEFFIT. *J. Synchrotron Radiat.* **2005**, *12*, 537–541. [CrossRef] [PubMed]
42. Graulis, S.; Daškevi, A.; Merkys, A.; Chateigner, D.; Lutterotti, L.; Quirós, M.; Serebryanaya, N.R.; Moeck, P.; Downs, R.T.; Le Bail, A. Crystallography Open Database (COD): An open-access collection of crystal structures and platform for world-wide collaboration. *Nucleic Acids Res.* **2012**, *40*, D420–D427. [CrossRef] [PubMed]
43. Lokesh, S.; Kim, J.; Zhou, Y.; Wu, D.; Pan, B.; Wang, X.; Behrens, S.; Huang, C.-H.; Yang, Y. Anaerobic Dehalogenation by Reduced Aqueous Biochars. *Environ. Sci. Technol.* **2020**, *54*, 15142–15150. [CrossRef] [PubMed]
44. Adhikari, D.; Sowers, T.; Stuckey, J.W.; Wang, X.; Sparks, D.L.; Yang, Y. Formation and redox reactivity of ferrihydrite-organic carbon-calcium co-precipitates. *Geochim. Cosmochim. Acta* **2019**, *244*, 86–98. [CrossRef]
45. Yang, G.; Wang, Z.; Xian, Q.; Shen, F.; Sun, C.; Zhang, Y.; Wu, J. Effects of pyrolysis temperature on the physicochemical properties of biochar derived from vermicompost and its potential use as an environmental amendment. *RSC Adv.* **2015**, *5*, 4117–4125. [CrossRef]

46. Agbeshie, A.A.; Abugre, S.; Atta-Darkwa, T.; Awuah, R. A review of the effects of forest fire on soil properties. *J. For. Res.* **2022**, *33*, 1419–1441. [[CrossRef](#)]
47. Sigmund, G.; Santin, C.; Pignitter, M.; Tepe, N.; Doerr, S.H.; Hofmann, T. Environmentally persistent free radicals are ubiquitous in wildfire charcoals and remain stable for years. *Commun. Earth Environ.* **2021**, *2*, 68. [[CrossRef](#)]
48. Kluepfel, L.; Keiluweit, M.; Kleber, M.; Sander, M. Redox Properties of Plant Biomass-Derived Black Carbon (Biochar). *Environ. Sci. Technol.* **2014**, *48*, 5601–5611. [[CrossRef](#)] [[PubMed](#)]
49. Uchimiya, M.; Stone, A.T. Reversible redox chemistry of quinones: Impact on biogeochemical cycles. *Chemosphere* **2009**, *77*, 451–458. [[CrossRef](#)] [[PubMed](#)]
50. Scott, D.T.; McKnight, D.M.; Blunt-Harris, E.L.; Kolesar, S.E.; Lovley, D.R. Quinone moieties act as electron acceptors in the reduction of humic substances by humics-reducing microorganisms. *Environ. Sci. Technol.* **1998**, *32*, 2984–2989. [[CrossRef](#)]
51. Lokesh, S.; Lard, M.L.; Cook, R.L.; Yang, Y. Critical Role of Semiquinones in Reductive Dehalogenation. *Environ. Sci. Technol.* **2023**, *57*, 14218–14225. [[CrossRef](#)] [[PubMed](#)]
52. Bento-Gonçalves, A.; Vieira, A.; Ubeda, X.; Martin, D. Fire and soils: Key concepts and recent advances. *Geoderma* **2012**, *191*, 3–13. [[CrossRef](#)]
53. Johnston, S.G.; Karimian, N.; Burton, E.D. Fire Promotes Arsenic Mobilization and Rapid Arsenic(III) Formation in Soil via Thermal Alteration of Arsenic-Bearing Iron Oxides. *Front. Earth Sci.* **2019**, *7*, 463230. [[CrossRef](#)]
54. Uchimiya, M.; Wartelle, L.H.; Klasson, K.T.; Fortier, C.A.; Lima, I.M. Influence of Pyrolysis Temperature on Biochar Property and Function as a Heavy Metal Sorbent in Soil. *J. Agric. Food Chem.* **2011**, *59*, 2501–2510. [[CrossRef](#)]
55. Hall, S.J.; Silver, W.L.; Timokhin, V.I.; Hammel, K.E. Iron addition to soil specifically stabilized lignin. *Soil Biol. Biochem.* **2016**, *98*, 95–98. [[CrossRef](#)]
56. Xu, W.Q.; Walpen, N.; Keiluweit, M.; Kleber, M.; Sander, M. Redox Properties of Pyrogenic Dissolved Organic Matter (pyDOM) from Biomass-Derived Chars. *Environ. Sci. Technol.* **2021**, *55*, 11434–11444. [[CrossRef](#)]
57. Hurteau, M.D.; Westerling, A.L.; Wiedinmyer, C.; Bryant, B.P. Projected Effects of Climate and Development on California Wildfire Emissions through 2100. *Environ. Sci. Technol.* **2014**, *48*, 2298–2304. [[CrossRef](#)]
58. Loudermilk, E.L.; Stanton, A.; Scheller, R.M.; Dilts, T.E.; Weisberg, P.J.; Skinner, C.; Yang, J. Effectiveness of fuel treatments for mitigating wildfire risk and sequestering forest carbon: A case study in the Lake Tahoe Basin. *For. Ecol. Manag.* **2014**, *323*, 114–125. [[CrossRef](#)]
59. Bisiaux, M.M.; Edwards, R.; Heyvaert, A.C.; Thomas, J.M.; Fitzgerald, B.; Susfalk, R.B.; Schladow, S.G.; Thaw, M. Stormwater and Fire as Sources of Black Carbon Nanoparticles to Lake Tahoe. *Environ. Sci. Technol.* **2011**, *45*, 2065–2071. [[CrossRef](#)]
60. Heron, T.; Strawn, D.G.; Dobre, M.; Cade-Menun, B.J.; Deval, C.; Brooks, E.S.; Piaskowski, J.; Gasch, C.; Crump, A. Soil Phosphorus Speciation and Availability in Meadows and Forests in Alpine Lake Watersheds with Different Parent Materials. *Front. For. Glob. Change* **2021**, *3*, 604200. [[CrossRef](#)]
61. Goldberg, S.J.; Ball, G.I.; Allen, B.C.; Schladow, S.G.; Simpson, A.J.; Masoom, H.; Soong, R.; Graven, H.D.; Aluwihare, L.I. Refractory dissolved organic nitrogen accumulation in high-elevation lakes. *Nat. Commun.* **2015**, *6*, 6347. [[CrossRef](#)]

Disclaimer/Publisher’s Note: The statements, opinions and data contained in all publications are solely those of the individual author(s) and contributor(s) and not of MDPI and/or the editor(s). MDPI and/or the editor(s) disclaim responsibility for any injury to people or property resulting from any ideas, methods, instructions or products referred to in the content.